ENGINEERING CHARACTERISTICS OF NEAR FAULT GROUND MOTION

Paul Somerville
Woodward-Clyde, Pasadena, CA

ABSTRACT

This paper explains the effects of rupture directivity on near-fault ground motions, describes an empirical model of these effects, provides guidelines for the specification of response spectra and time histories to represent near-fault ground motions, and provides guidelines for the selection of time histories.

INTRODUCTION

An earthquake is a shear dislocation that begins at a point on a fault and spreads at a velocity that is almost as large as the shear wave velocity. The propagation of fault rupture toward a site at very high velocity causes most of the seismic energy from the rupture to arrive in a single large long period pulse of motion which occurs at the beginning of the record (Somerville and Graves, 1993). This pulse of motion, sometimes referred to as "fling," represents the cumulative effect of almost all of the seismic radiation from the fault. The radiation pattern of the shear dislocation on the fault causes this large pulse of motion to be oriented in the direction perpendicular to the fault, causing the strike-normal peak velocity to be larger than the strike-parallel peak velocity. The effect of forward rupture directivity on the response spectrum is to increase the level of the response spectrum of the horizontal component normal to the fault strike at periods longer than 0.5 seconds. This causes the peak response spectral acceleration of the strike-normal component to shift to longer periods, for example from 0.25 seconds to as much as 0.75 seconds. Near fault effects cannot be adequately described by uniform scaling of a fixed response spectral shape; the shape of the spectrum must become richer in long periods as the level of the spectrum increases. Figure 1 shows these effects of rupture directivity in the time history and response spectrum of the Rinaldi recording of the 1994 Northridge earthquake.

Forward rupture directivity effects occur when two conditions are met: the rupture front propagates toward the site, and the direction of slip on the fault is aligned with the site. The conditions for generating forward rupture directivity effects are readily met in strike-slip faulting, where the fault slip direction is oriented horizontally in the direction along the strike of the fault, and rupture propagates horizontally along strike either unilaterally or bilaterally. However, not all near-fault locations experience forward rupture directivity effects in a given event. Backward directivity effects, which occur when the rupture propagates away from the site, give rise to the opposite effect: long duration motions having low amplitudes at long periods. This is illustrated in Figure 2, which shows the directivity effect in strike-slip faulting using the strike-normal components of ground velocity from two near-fault recordings of the magnitude 7.3 Landers earthquake of 1992 (Wald and Heaton, 1994). The Lucerne record, which is located 1.1 km from the surface rupture and 45 km from the epicenter of the Landers earthquake, consists of a large, brief pulse of motion (due to forward directivity effects), while the Joshua Tree record, located near the epicenter, consists of a long duration, low amplitude record (due to backward directivity effects).

The conditions required for forward directivity are also met in dip slip faulting, including both reverse and normal faults. The alignment of both the rupture direction and the slip direction up the fault plane produces rupture directivity effects at sites located around the surface exposure of the fault (or its updip projection if it does not break the surface). Consequently, it is generally the case that all sites located near the surface exposure of a dip-slip-fault experience forward rupture directivity when an earthquake occurs on that fault. Unlike the case for strike-slip faulting, where we expect forward rupture directivity effects to be most concentrated away from the hypocenter, dip slip faulting produces directivity effects on the ground surface that are most concentrated updip from the hypocenter. Recordings of the 1994 Northridge earthquake from the northern margin of the San Fernando Valley, such as the one at Rinaldi shown in Figure 1, contain forward rupture directivity effects.

EMPIRICAL MODEL OF NEAR-FAULT GROUND MOTIONS

Somerville et al. (1997) used a large set of near fault strong motion recordings to develop a quantitative model of rupture directivity effects. This model can be used to modify existing ground motion attenuation relations to incorporate directivity effects in ground motions used for seismic design. The ground motion parameters that are modified for directivity effects include the average horizontal response spectral acceleration; the average duration of the two horizontal acceleration time histories; and the ratio of strike normal to strike parallel spectral acceleration. *Strike-normal* refers to the horizontal component of motion *normal* to the strike of the fault. *Strike-parallel* refers to the horizontal component of motion *parallel* to the strike of the fault. Following the method of Husid (1969), duration is defined as the time between 5% and 75% of the cumulative squared acceleration, following the convention of Abrahamson and Silva (1997b).

In this model, amplitude variations due to rupture directivity depend on two geometrical parameters. First, the smaller the angle between the direction of rupture propagation and the direction of waves travelling from the fault to the site, the larger the amplitude. Second, the larger the fraction of the fault rupture surface that lies between the hypocenter and the site, the larger the amplitude. The duration of strong motion is modeled using the same two parameters, with an inverse relationship between duration and amplitude. The azimuth and zenith angles and length and width ratios are illustrated for strike-slip and dip-slip faulting in Figure 3. For strike-slip faults, the angle θ and length ratio X are measured from the epicenter to the site in the horizontal plane. For dip-slip faults, the angle ϕ and width ratio Y are measured from the hypocenter to the site in the vertical plane oriented normal to the fault.

The effects of rupture directivity on ground motion amplitudes and duration are modeled using the function X cos θ for strike-slip faults and Y cos ϕ for dip-slip faults. For strike-slip faults, the variation of ground motion parameters with θ is independent of the distance from the rupture, r_{rup}. However, between the ends of a dip-slip fault, the variation of ground motion parameters with ϕ is indistinguishable from its variation with rupture distance r_{rup}. Since rupture distance is a primary ground motion parameter already included in attenuation relations, we find more spatial variability of strike-slip motions with cos θ than of dip-slip motions with cos ϕ. The strike normal to strike parallel ratio was modeled using a cos 2ξ dependence of the strike normal to strike parallel ratio, where ξ is θ for strike-slip and ϕ for dip-slip in the range of 0 to 45 degrees.

The dependence of the spectral amplification factor on X cos θ for strike-slip faulting and Y cos ϕ for dip-slip faulting is shown in Figure 4a. These effects begin at 0.6 seconds period

and increase with period. For strike-slip faulting, maximum directivity conditions (X cos θ = 1) cause an amplitude about 1.8 times larger than average at 2 seconds period, while minimum directivity effects cause an amplitude about 0.6 times average. In the model for dip-slip faulting, which excludes sites off the ends of the fault as shown in Figure 3, the effects lie in the range of about 1.2 to 0.8.

The dependence of the duration factor on X cos θ for strike-slip faulting and on Y cos ϕ for dip-slip faulting is shown in Figure 4b. As expected, there is an inverse correlation between duration residuals and amplitude residuals. For maximum directivity conditions (X cos θ or Y cos ϕ = 1), the duration is about 0.55 times the average duration for both strike-slip and dip-slip faulting. For minimum directivity conditions, the ground motion durations are 2.1 and 1.6 times longer than average for dip-slip and strike-slip faulting respectively.

The model of the strike-normal to average horizontal ratio, which is independent of faulting mechanism, is displayed in Figure 5. The top part of the figure shows the period dependence of the ratio for various magnitudes and distances, and the bottom part of the figure shows the distance dependence of the ratio for various magnitudes and periods, averaged over all values of the angles θ and ϕ. The strike-normal motion is obtained by multiplying the attenuation relation value by the strike-normal to average horizontal ratio, and the strike-parallel motion is obtained by dividing the attenuation relation value by this ratio. The bottom right part of the figure shows the dependence of the ratio on θ or ϕ for M = 7 and r_{rup} = 5 as a function of period. The period dependence of the ratio indicates a transition, at a period of about 0.6 seconds, from coherent source radiation and wave propagation conditions at long periods to incoherent source radiation and wave propagation conditions at short periods.

SPECIFICATION OF RESPONSE SPECTRA FOR NEAR-FAULT GROUND MOTIONS

Scenario Earthquake Approach

The ground motions used in the design or evaluation of a structure are usually specified in the form of a response spectrum or set of response spectra. In some instances, the response spectrum may represent a specified earthquake magnitude and distance. In California, seismic design criteria for dams and bridges are specified in whole or in part in this way. Until recently, the state of practice was to assume that near-fault effects are adequately represented in empirical ground motion models that are used to estimate the response spectrum for the specified magnitude and distance. The ground motions predicted by these empirical models represent the average of all rupture directivity conditions: forward, backward and neutral. However, ground motions influenced by forward rupture directivity are much larger than those for average rupture directivity for periods longer than 0.5 seconds. Since forward directivity has a high likelihood of occurring at any near-fault site, it may be appropriate to include forward rupture directivity as a criterion for the development of ground motions for the maximum credible event. The common practice of using the 84th percentile ground motion instead of the mean may in part accomplish this objective.

During the past 5 years, response spectra for the design of retrofits of Caltrans toll bridges have contained modifications of these empirical models to incorporate near-fault effects. These modifications consist of increasing the response spectrum level of the average horizontal component of ground motion at periods longer than 1 second, and specifying separate response spectra for the strike-normal and strike-parallel components of motion, using models such as that

described by Somerville et al. (1995). These modifications provide a response spectrum that is more nearly representative of forward rupture directivity effects. To date, Caltrans is the only organization that has adopted the use of different response spectra in the strike-normal and strike-parallel directions.

Modifications to the response spectral level have been included in the SEAOC Strength Code Change (SEAOC, 1996) in the form of the near source factor N. This factor modifies the basic response spectrum using factors N_a and N_v that depend on the distance to the fault, the slip rate of the fault, and the maximum magnitude that the fault can generate. At distances close to major active faults in California, the design values ("maximum considered") ground motion map in the 1997 NEHRP provisions (Building Seismic Safety Council, 1996) was also developed using near-fault factors applied to a standard seismic zone 4 response spectrum.

In Figure 6 we compare response spectra for the same earthquake (magnitude 7 strike-slip, distance 5 km, stiff soil conditions) but two different rupture directivity conditions. The spectra at the top are for average rupture directivity conditions (sites located randomly around the fault), while the spectra at the bottom are for forward rupture directivity conditions (where rupture propagates towards the site). In each case, we show the strike-normal, strike-parallel, and average horizontal response spectra based on the model of Somerville (1996). For comparison, we show proposed 1997 SEAOC code spectra including the near-fault factor for the appropriate source category (B) and site category (S_D). We use the "design basis" spectrum for comparison with average rupture directivity conditions, and the "maximum capable" spectrum from the base isolation part of the code (a factor of 1.25 higher) for comparison with forward rupture directivity conditions. The modifications for rupture directivity effects in Somerville (1996) are based not on the general model described above, but on a model derived from ten recordings at close distances to the 1989 Loma Prieta, 1994 Northridge, and 1995 Kobe earthquakes. This model has larger modifications than the general model for periods between 0.5 and 2.0 seconds.

The model for average directivity conditions shown at the top of Figure 6 does not change the average horizontal spectrum given by the empirical model (Abrahamson and Silva, 1997), but gives a strike-normal component that is larger and a strike-parallel component that is smaller. The model for forward directivity conditions, shown at the bottom of Figure 6, not only has a larger difference between these two components, but also increases the average horizontal component above that given by the empirical attenuation relation. The combination of these two modifications for forward directivity conditions results in the strike normal motion being about 2 times higher than the average given by the empirical attenuation relation for periods longer than about 0.5 second, and the strike parallel motion being about the same as the average given by the empirical attenuation relation.

Comparing the response spectral models at the top and bottom of Figure 6, we see that the most important effect of forward rupture directivity on the response spectrum is to increase the level of the response spectrum at periods longer than 0.5 seconds. This is manifested in a shift in the peak of response spectral acceleration from 0.3 seconds (which is also the peak for the strike parallel component) to 0.5 seconds for the average of the horizontal components and to 0.75 for the strike normal component. This indicates that near fault effects cannot be adequately described by uniform scaling of a fixed response spectral shape; the shape of the spectrum must become richer in long periods as the level of the spectrum increases. This has been implemented in the proposed 1997 SEAOC code change by using separate near-fault factors N_a and N_v for the acceleration and velocity parts of the code response spectrum.

The "design basis" spectrum at the top of Figure 6 envelopes both the strike-normal and strike-parallel components of motion for average directivity. However, the "maximum capable" spectrum at the bottom of Figure 6 lies below the strike-normal component for forward rupture directivity. Should engineers be concerned about the possibility of the strike-normal component exceeding the design criterion? There are two reasons for thinking that the answer is yes. First, recent destructive earthquakes have shown evidence of near-fault damage occurring in preferred directions that correspond to the strike-normal direction (north-south in the 1994 Northridge earthquake; northwest-southeast in the 1995 Kobe earthquake). Second, the difference between strike-normal and average motions is statistically significant close to large earthquakes. For example, in the case shown in the lower part of Figure 6, (forward rupture directivity at a distance of 5 km from a magnitude 7 earthquake), the strike-normal component is a factor of 1.4 times larger than the average horizontal component at long periods, with a standard error of a factor of 1.28.

In Figure 7, we compare the near-fault spectra for average (top) and forward (bottom) directivity conditions with the ground motion model of Abrahamson and Silva (1997) from which they were modified. For periods longer than about 0.75 second, the strike normal component for forward rupture directivity is about 25% larger than the 84th percentile ground motion for the average of the two horizontal components for average rupture directivity conditions, as given by the Abrahamson and Silva (1995) model. This indicates that use of the 84th percentile may partly if not completely accommodate the ground motion level in the strike normal direction for forward rupture directivity conditions.

Since fault strike is usually well known close to major faults, it is straighforward to take the difference between the strike normal and strike parallel components of motion into account in the evaluation of near-fault ground motions, especially for base isolated buildings, bridges, dams, and other structures that are particularly sensitive to long-period ground motions. Consideration of these differences may be especially important for the retrofit of existing structures near active faults (e.g. Salah-Mars et al., 1994). For new structures, the stronger ground motion in the strike normal direction could be accommodated by orienting the structure with its long axis normal to the fault, as shown in Figure 8. The implications of the orientation of dams with respect to fault-controlled valleys and range fronts for the specification of design ground motions have been described by Somerville and Graves (1996). Even if the specific location and orientation of faults is not known, there may be a high enough level of certainty in the strike of faults in a region (for example, of blind thrust faults in the Los Angeles basin) to warrant consideration of larger strike-normal ground motions.

Probabilistic Approach

In many instances, the response spectrum is defined probabilistically as that having a specified annual probability of exceedance. A probabilistic response spectrum contains contributions from the entire range of magnitude-distance pairs that affect the site. This is the approach that is used to generate response spectra using the site-specific method prescribed by the UBC. It is also the approach used by the USGS to generate the National Seismic Hazard Maps. The "maximum capable" ground motion used in the base isolation code is associated with a specified probability of occurrence (10% in 100 years), and ground motion criteria for bridges and dams are also informally associated with annual probabilities of occurrence.

The current state of practice in the development of probabilistic response spectra is to assume that near-fault effects are adequately represented in the empirical ground motion models that are used to estimate the response spectrum for the specified magnitude and distance. However, the means now exist to incorporate near-fault effects in a more specific way by using the empirical model of Somerville et al. (1997) which is summarized in Figures 4 and 5. This model can be implemented by randomizing the location of the hypocenter on the fault planes of earthquakes having magnitudes larger than 6. The model has not yet been implemented in a probabilistic seismic hazard analysis. However, the main anticipated effect is a larger strike-normal response spectrum and a smaller strike-parallel response spectrum than the average horizontal spectrum estimated by current methods. At low probabilities, there may also be some increase in the average response spectrum due to the larger variability in ground motions predicted by the model.

SPECIFICATION OF TIME HISTORIES FOR NEAR-FAULT GROUND MOTIONS

Design and analysis of large structures is often done using time histories that are representative of the design response spectrum. The time histories, which may be from recorded earthquakes or from strong motion simulations of the kind described below, are sometimes spectrally matched to a design response spectrum. The modifications that we have developed to incorporate rupture directivity effects in the response spectrum are not sufficient to ensure the appropriate incorporation of rupture directivity effects in time histories that are matched to these spectra. This is because the forward rupture directivity effect is manifested in the time domain by a large pulse of long period ground motion, and the spectral matching process cannot build a rupture directivity pulse into a record where none is present to begin with. Forward rupture directivity effects are present in some but not all near-fault strong motion recordings. Since the response spectrum developed for design or evaluation of a near-fault site will be influenced by forward rupture directivity effects at most sites, it is important to select an appropriate proportion of time histories that include forward rupture directivity effects if time histories are being used to represent the response spectrum.

Orientation of Time Histories

If it is desired to fully represent near-fault conditions in the time histories, then it is necessary to initially specify the strike-normal and strike-parallel components of the time histories. If the axis of the structure is aligned at some angle θ to the strike of the fault, then the longitudinal and transverse time histories should then be derived from the strike-normal (SN) and strike-parallel (SP) time histories using the following equation:

$$\text{long} = SP \cos\theta + SN \sin\theta$$
$$\text{trans} = SP \sin\theta - SN \cos\theta$$

In Figure 8a, we schematically illustrate the recording of strong motion near fault A on the north and east components, the rotation of the north and east to strike-normal and strike-parallel, the transposition of the strike-normal and strike-parallel components to the structure site near fault B, and the rotation of the strike-normal and strike-parallel components into longitudinal and transverse components at the structure site. To avoid the first rotation step, we should archive near-fault strong motion recordings and simulations in their strike-normal and strike-parallel components.

Although near-fault ground displacements contain permanent displacements due to the static displacement field of the earthquake, analog systems traditionally used to record strong motion do not retain these displacements, and in any case they are removed by highpass filtering in traditional processing methods. However, in some cases the permanent ground displacements may be significant for design, and in these cases it is important to specify the correct orientation of the static and dynamic ground displacements. In Figure 8b, we show the sense of motion of the permanent ground displacement near left-lateral and right-lateral unilateral strike-slip faults for rupture propagation in either direction (that is, for epicenters at either end of the fault). The sense of strike normal displacement is continuous across the fault, whereas the sense of strike parallel displacement is discontinuous across the fault (reflecting the displacement on the fault). For a given sense of slip (e.g. strike-slip), the polarity of the strike parallel displacement is the same for rupture in either direction, but the polarity of the strike normal displacement is opposite for rupture in opposite directions. Current building codes assume that the two horizontal components are uncorrelated, and prescribe interchanging the two horizontal components in structural analyses. This is clearly inappropriate for near-fault ground motions, in which there are systematic differences between the strike-normal and strike-parallel components. Interchanging the components can represent physically unrealizable scenarios given the known orientation of the fault.

Scenario Earthquake Approach

If the response spectrum is derived from a scenario earthquake, then the magnitude and distance of the earthquake are specified, and time histories representative of that magnitude and distance need to be selected. If the response spectrum is based on the median level ground motion, then it represents average directivity conditions, and it is appropriate to select time histories that span a range of directivity conditions. However, if the response spectrum is based on the mean plus one standard deviation ground motion level, then it represents forward directivity conditions, and most if not all of the time histories should be for forward rupture directivity conditions. As described in Figure 7, the strike normal ground motion level for forward rupture directivity conditions is about as large as or larger than the 84th percentile response spectrum for average directivity conditions.

With the exception of Caltrans toll bridges noted above, design or analysis response spectra apply to the average of the two horizontal components of ground motion. When scaling a time history to match this spectrum, a scaling factor should be found that matches the average of the two horizontal components of the time history to the design spectrum. This factor should then be applied to each of the two horizontal components in order to leave unchanged the ratio between the two horizontal components. In the case when the response spectra of the strike-normal and strike-parallel components of motion are separately specified (e.g. for Caltrans toll bridges), then the time histories can be scaled separately to these response spectra.

Probabilistic Approach

A probabilistic seismic hazard analysis (PSHA) takes into account the ground motions from the full range of earthquake magnitudes that can occur on each fault or source zone that can affect the site. The time histories that are selected must represent the dominant combinations of magnitude, distance and ϵ that contribute to the response spectrum. The parameter ϵ is defined as the number of standard deviations above or below the median ground motion level for that magnitude and distance that is required to match the probabilistic spectrum. The magnitude,

distance and ϵ combinations are identified through deaggregation of the seismic hazard (McGuire, 1995; Silva and Toro, 1996).

If the probabilistic seismic hazard analysis were to include the near-fault modifications for rupture directivity effects described above, then the deaggregation could include values of the directivity function X cos θ for strike-slip faults and Y cos ϕ for dip-slip faults, and the directivity content of time histories could be selected based on the predominant value of the directivity function. Otherwise, some estimate of the appropriate directivity content of the time histories can be obtained from the parameter ϵ defined above. If the predominant value of ϵ is near zero, then the response spectrum approximately represents average directivity conditions, and it is appropriate to select time histories that span a range of directivity conditions. However, if the predominant value of ϵ is one, then the response spectrum is at the mean plus one standard deviation ground motion level for that event, representing forward directivity conditions, and most if not all of the time histories should be for forward rupture directivity conditions. In the deaggregation of seismic hazard at 10% probability of exceedance in 50 years in Los Angeles and San Francisco, Silva and Toro (1996) found that the ϵ value was approximately one on average for the predominant contribution to the hazard. This indicates the need to select time histories having predominantly forward rupture directivity conditions in order to represent the 10% in 50 year ground motions in Los Angeles and San Francisco.

SELECTION OF TIME HISTORIES FOR NEAR-FAULT GROUND MOTIONS

If time histories are used in conjunction with the response spectrum, it is important to select time histories which appropriately include rupture directivity effects because the spectral matching process cannot build a rupture directivity pulse into a record where none is present to begin with. As a guide to the selection of time histories for use in design and evaluation of structures that are sensitive to long-period ground motions, we have listed a set of near-fault strong motion recordings and indicated the nature of the rupture directivity effects that they contain. The catalog of records given in Table 1 includes those whose closest distance to the fault rupture is 10 km or less in the data set that was used by Somerville et al. (1995, 1997) to develop an empirical model of directivity effects on strong ground motions. The influence of rupture directivity effects on each record is indicated, based on the geometrical relationships between the recording site, the fault rupture, the epicenter, and the direction of slip on the fault. The table lists the peak horizontal accelerations and velocities of the records in the strike normal and strike parallel directions. This table can complement the extensive classification and evaluation of earthquake records using a range of ground motion parameters provided by Naeim and Anderson (1993; 1996).

The recorded time histories listed in Table 1 include a limited number of recordings at close distances to large earthquakes. Broadband simulation techniques which have been validated against recorded strong ground motions can be used to generate time histories for large magnitudes and close distances. For example, broadband time histories for hypothesized magnitude 7 earthquakes on the Elysian Park thrust beneath downtown Los Angeles (Somerville et al., 1995), and on the predominantly strike-slip Palos Verdes fault in the Long Beach area, were used by Somerville, Smith and Sun (1997) to complement recorded ground motions in a set of near fault recordings for use in Phase 2 of the SAC Steel Project. Both the recorded and simulated near-fault time histories can be accessed by anonymous ftp to "ftp.csn.net" in the directory wwclyde/SAC2, file NearFault. They are rotated into strike-normal and strike-parallel components.

We conclude this paper with some specific guidelines for the selection of appropriate time histories for the representation of near-fault rupture directivity effects.

Forward Rupture Directivity

Forward directivity occurs when the rupture propagates toward the site and the direction of slip on the fault is also toward the site. Most near-fault strike-slip recordings, and all near-fault reverse fault recordings, are influenced by forward directivity. Backward directivity occurs when the rupture propagates away from the site. Recordings near the epicenters of strike-slip earthquakes, a relatively small group, fall in the backward directivity category. None of the reverse faults in our data set ruptured in the downdip direction away from surface stations, so none have backward directivity. Recordings that do not clearly belong in either of these categories are grouped in a neutral category. This category includes sites located fairly close to the epicenters of strike-slip earthquakes, and sites located off the end of the updip projection of reverse faults.

Recordings Close to Epicenters

It is a common fallacy to assume that recordings close to the epicenters of strike-slip and oblique-slip earthquakes (such as Bond's Corner, 1971 Imperial Valley earthquake; Corralitos, 1987 Loma Prieta earthquake; and Joshua Tree, 1992 Landers earthquake) contain forward rupture directivity effects. On the contrary, these records contain neutral or backward directivity effects, produced when the rupture propagates away from the site, and are characterized by relatively low amplitudes of long period ground motions. Also, strong motion recordings above shallow thrust faults, such as the Cape Mendocino and Petrolia recordings of the 1992 Cape Mendocino earthquake, do not contain rupture directivity effects. The effects of rupture directivity are primarily manifested at the longer periods, so that large peak accelerations in near-fault recordings do not necessarily imply large long period ground motions.

Faulting Mechanism

If the seismic hazard at a site is dominated by a particular style of faulting of faulting mechanism (e.g. strike-slip or reverse), it is preferable to use time histories from that style of faulting. In the recorded data analyzed by Somerville et al. (1997), it was found that the relation between strike-normal and strike-parallel ground motions is similar for strike-slip and reverse earthquakes. However, differences between strike-slip and reverse faulting were found in the azimuthal variation of duration and response spectral amplification. Also, for larger earthquakes, there may be differences between strike-slip and reverse ground motions because the rupture directivity effect in reverse faulting builds up over a limited fault width, whereas for strike-slip faulting it can build up over a much larger fault length.

Duration

It is a common fallacy to assume that near-fault ground motion time histories close to large earthquakes should have a long duration. As shown in Figure 4b, the stronger the near-fault directivity effect, the shorter the duration. This is because the forward directivity effect causes nearly all of the seismic radation from the fault to arrive in a single brief pulse of motion. It does not make sense to sequentially combine several near-fault records containing brief pulses to make up for the short duration that is characteristic of forward rupture directivity effects.

REFERENCES

Abrahamson. N.A. and W.J. Silva (1997). Empirical response spectral attenuation relations for shallow crustal earthquakes, *Seismological Research Letters* 68, 94-127.

McGuire, R.K. (1995). Probabilistic seismic hazard analysis and design earthquakes: closing the loop. *Bull. Seism. Soc. Am.* 86, 1275-1284.

Naeim, F. (1995). On seismic design implications of the 1994 Northridge earthquake records, *Earthquake Spectra* 11, 91-110.

Naeim, F. and J.C. Anderson (1993). Classification and evaluation of earthquake records for design, *Earthquake Engineering Research Institute*, 287 pp.

Naeim, F. and J.C. Anderson (1996). Design Classification of Horizontal and Vertical Earthquake Ground Motion, *Report to the U.S. Geological Survey by John. A. Martin & Associates, Inc.., JAMA Report No. 7738.68-96, 427 pp.*

Salah-Mars, S., L.H. Mejia, P.G. Somerville, R.K. Green, R.O. Hamburger, and C.A. Cole (1994). Ground motions for base isolation seismic retrofit of a building near the Hayward fault, *Proceedings of the 5th U.S. National Conference on Earthquake Engineering,* Chicago, July 1994.

Silva, W. and G. Toro (1996). Verification of response spectral shapes and anchor points for different site categories for building design codes. SMIP96 Seminar on Seismological and Engineering Implications of Recent Strong Motion Data, p. 37-51.

Somerville, P.G., N.F. Smith, R.W. Graves, and N.A. Abrahamson (1997). Modification of empirical strong ground motion attenuation relations to include the amplitude and duration effects of rupture directivity, *Seismological Research Letters* 68, 199-222.

Somerville, P.G. (1996). Strong ground motions of the Kobe, Japan earthquake of Jan. 17, 1995, and development of a model of forward rupture directivity effects applicable in California. *Proceedings of the Western Regional Technical Seminar on Earthquake Engineering for Dams,* Association of State Dam Safety Officials, Sacramento, April 11-12, 1996.

Somerville, P.G., N.F. Smith, R.W. Graves, and N.A. Abrahamson (1995a). Representation of near-fault rupture directivity effects in design ground motions, and application to Caltrans bridges. *Proceedings of the National Seismic Conference on Bridges and Highways,* San Diego, December 10-13, 1995.

Somerville, P.G., R.W. Graves, and C.K. Saikia (1995b). Characterization of Ground Motions During the Northridge Earthquake of January 17, 1994. Report No. SAC 95-03 of the SAC Joint Venture.

Somerville, Smith and Sun (1997). Suites of ground motion time histories developed for Phase 2 of the SAC Steel Project. Unpublished draft report.

Table 1. Description of Rupture Directivity Effects in Near-Fault Strong Motion Recordings
(See Table 8 of Somerville et al., 1997 for a listing that includes directivity parameters X and θ for strike-slip faults, and ϕ and Y for dip-slip faults, in place of the general directivity descriptor [forward, neutral, backward] provided in this table).

EQK DATE	STAT. NO.	STATION	CLOSEST DISTANCE (km)	SITE CODE[1]	PEAK HORIZONTAL ACCEL (g)		PEAK HORIZONTAL VEL (cm/s)		DIRECTIVITY[3]
					FN[2]	FP[2]	FN[2]	FP[2]	
400519	117	IMPERIAL VAL IRRIG. DIST, EL CENTRO	10.0	SL	0.21	0.32	32.2	60.1	B
660627	014	CHOLAME, SHANDON, CA ARY 5	3.7	SL	0.33	0.36	26.1	23.6	F
660627	015	CHOLAME, SHANDON, CA ARY 8	8.0	SL	0.24	0.28	11.7	12.2	F
660627	097	TEMBLOR, CA, STATION 2	4.4	HR	0.36	0.25	23.5	12.6	F
671210	9001	KOYNA DAM	3.0	HR	0.51	0.45	32.9	21.9	B
710209	24207	PACOIMA DAM	3.3	HR	1.17	1.08	114.9	59.3	F
760517	9201	KARAKYR POINT, USSR	3.0	SR	0.65	0.67	63.7	59.8	N
780916	9101	TABAS	1.2	SR	0.90	0.98	110.2	106.7	N
791015	6616	AEROPUERTO MEXICALI	0.4	SL	0.28	0.36	27.1	42.7	B
791015	6618	AGRARIAS	0.8	SL	0.24	0.36	38.7	39.7	B
791015	955	EL CENTRO ARY 4, ANDERSON ROAD	7.1	SL	0.36	0.49	77.7	38.0	F
791015	952	EL CENTRO ARY 5, JAMES ROAD	4.1	SL	0.37	0.53	88.1	43.8	F
791015	942	EL CENTRO ARY 6, HUSTON ROAD	1.2	SL	0.43	0.35	106.2	62.9	F
791015	5028	EL CENTRO ARY 7, IMPERIAL VAL COLL.	0.2	SL	0.46	0.33	106.4	44.7	F
791015	958	EL CENTRO ARY 8, CRUICKSHANK RD	3.8	SL	0.47	0.61	50.1	52.7	F
791015	412	EL CENTRO ARY 10, HOSPITAL	9.0	SL	0.18	0.23	44.9	39.9	F
791015	5054	BONDS CORNER, EL CENTRO	2.4	SL	0.79	0.59	48.6	43.8	B
791015	5053	FIRE STATION, CALEXICO	10.1	SL	0.26	0.21	18.3	15.4	N
791015	6619	MEXICALI CASA FLORES	9.7	SL	0.23	0.43	19.3	28.8	B
791015	6622	COMPUERTAS	4.5	SL	0.15	0.15	9.7	13.7	B
791015	9301	EL CENTRO DIFFERENTIAL ARRAY 1	5.5	SL	0.73	0.74	119.8	111.8	F
791015	9302	EL CENTRO DIFFERENTIAL ARRAY 2	5.5	SL	0.62	0.77	121.6	110.4	F
791015	9304	EL CENTRO DIFFERENTIAL ARRAY 3	5.4	SL	0.61	0.68	120.8	109.5	F
791015	9305	EL CENTRO DIFFERENTIAL ARRAY 4	5.2	SL	0.83	0.73	117.9	104.4	F
791015	9306	EL CENTRO DIFFERENTIAL ARRAY 5	5.1	SL	1.19	2.07	131.4	135.7	F
791015	5165	DIFFERENTIAL ARRAY-DOGWOOD ROAD	5.2	SL	0.41	0.45	56.0	49.3	F
791015	5055	POST OFFICE, HOLTVILLE	7.5	SL	0.27	0.23	50.3	42.7	N
791015	335	IMPERIAL COUNTY FF	7.4	SL	0.18	0.22	52.1	41.3	F
840424	1652	ANDERSON DAM, DOWNSTREAM	4.5	SL	0.44	0.28	27.0	28.9	F
840424	57217	COYOTE LAKE DAM, SAN MARTIN	0.01	SR	0.85	0.93	66.5	68.3	F
840424	57191	HALLS VALLEY	2.5	SL	0.31	0.16	39.0	14.2	B
851223	6097	IVERSON, NW TERRITORIES (STA 1)	9.6	HR	1.24	1.20	45.3	44.1	N
851223	6098	SLIDE MOUNTAIN (STA 2)	6.1	HR	0.40	0.42	27.0	37.6	N

[1]HR-HARD ROCK; SR SEDIMENTARY AND CONGLOMERATED ROCK; SL-SOIL AND ALLUVIUM
[2]FN-FAULT NORMAL; FP-FAULT PARALLEL
[3]F-FORWARD; N-NEUTRAL; B-BACKWARD

Table 1 (cont.). Description of Rupture Directivity Effects in Near-Fault Strong Motion Recordings
(See Table 8 of Somerville et al., 1997 for a listing that includes directivity parameters X and θ for strike-slip faults, and ϕ and Y for dip-slip faults, in place of the general directivity descriptor [forward, neutral, backward] provided in this table).

EQK DATE	STAT. NO.	STATION	CLOSEST DISTANCE (km)	SITE CODE[1]	PEAK HORIZONTAL ACCEL (g)		PEAK HORIZONTAL VEL (cm/s)		DIRECTIVITY[3]
					FN[2]	FP[2]	FN[2]	FP[2]	
851223	6098	SLIDE MOUNTAIN (STA 2)	6.1	HR	0.40	0.42	27.0	37.6	N
860708	5073	CABAZON - POST OFFICE	8.4	SL	0.23	0.20	6.9	16.2	F
860708	12149	DESERT HOT SPRINGS	6.7	SL	0.34	0.29	29.7	22.9	N
860708	5997	DEVERS HILL SUBSTATION	4.1	SL	1.10	0.42	90.0	14.7	F
860708	5070	NORTH PALM SPRINGS POST OFFICE	4.0	SL	0.71	0.60	67.8	32.9	F
860708	12025	PALM SPRINGS AIRPORT	9.6	SL	0.16	0.15	14.7	10.3	F
860708	5072	WHITEWATER CANYON TROUT FARM	5.9	SL	0.50	0.58	39.6	29.9	F
891017	57007	CORRALITOS	3.4	SR	0.47	0.51	45.7	43.9	B
891017	47006	GAVILAN COLLEGE PHYS. SCI. BLDG.	9.5	SL	0.30	0.39	31.9	27.6	N
891017	47379	GILROY #1 - GAVILAN WATER TOWER	9.2	SR	0.42	0.41	39.5	29.8	N
891017	57180	LEXINGTON DAM - LEFT ABUTMENT	6.3	SR	0.45	0.39	118.0	45.6	F
891017		LOS GATOS PRESENTATION CNTR	3.5	HR	0.66	0.44	105.5	57.4	F
891017	58065	SARATOGA - ALOHA AVENUE	8.3	SL	0.37	0.35	57.0	44.8	F
920313	9401	ERZINCAN, TURKEY	2.0	SL	0.43	0.46	120.2	65.4	F
920628	22170	JOSHUA TREE - FIRE STATION	7.4	SL	0.28	0.19	42.7	30.0	B
920628		LUCERNE VALLEY	1.1	SL	0.76	0.73	127.5	95.3	F
940117	655	JENSEN FILTRATION PLANT	6.5	SL	0.38	0.62	45.4	100.1	F
940117	24088	PACOIMA; KAGEL CANYON	8.0	HR	0.53	0.24	55.5	36.8	N
940117	24279	NEWHALL; LA COUNTY FIRE STATION	6.7	SL	0.72	0.65	118.2	49.3	F
940117	24087	ARLETA; NORDHOFF FIRE STATION	9.5	SL	0.24	0.33	26.0	31.4	N
940117	24207	PACOIMA DAM - DOWNSTREAM	7.6	HR	0.50	0.24	48.5	18.9	F
940117	5968	RINALDI RECEIVING STATION - FF	7.5	SL	0.89	0.39	178.4	67.5	F
940117	306	SYLMAR CONVERTER STATION - FF	6.4	SL	0.59	0.80	130.1	89.3	F
940117	6273	SYLMAR CONVERTER STATION E - FF	6.2	SL	0.84	0.49	116.3	75.8	F
940117	637	SEPULVEDA VA HOSPITAL	9.3	SL	0.73	0.79	48.7	76.0	F
940117	24514	SYLMAR; OLIVE VIEW FF	6.2	SL	0.73	0.59	122.2	54.3	F
950117		KOBE UNIVERSITY (CEORKA)	3.8	RK	0.33	0.26	49.1	38.8	F
950117		KOBE (CEORKA)	6.2	SL	0.67	0.54	56.4	38.2	F
950117		KOBE (JMA)	3.4	SL	0.86	0.52	104.3	51.9	F
950117		KOBE PORT ISLAND, SURFACE	6.6	SL	0.43	0.14	95.9	30.3	F
950117		TAKATORI (JR)	4.3	SL	0.81	0.42	174.9	62.7	F

[1]HR-HARD ROCK; SR-SEDIMENTARY AND CONGLOMERATE ROCK; SL-SOIL AND ALLUVIUM
[2]FN-FAULT NORMAL; FP-FAULT PARALLEL
[3]F-FORWARD; N-NEUTRAL; B-BACKWARD

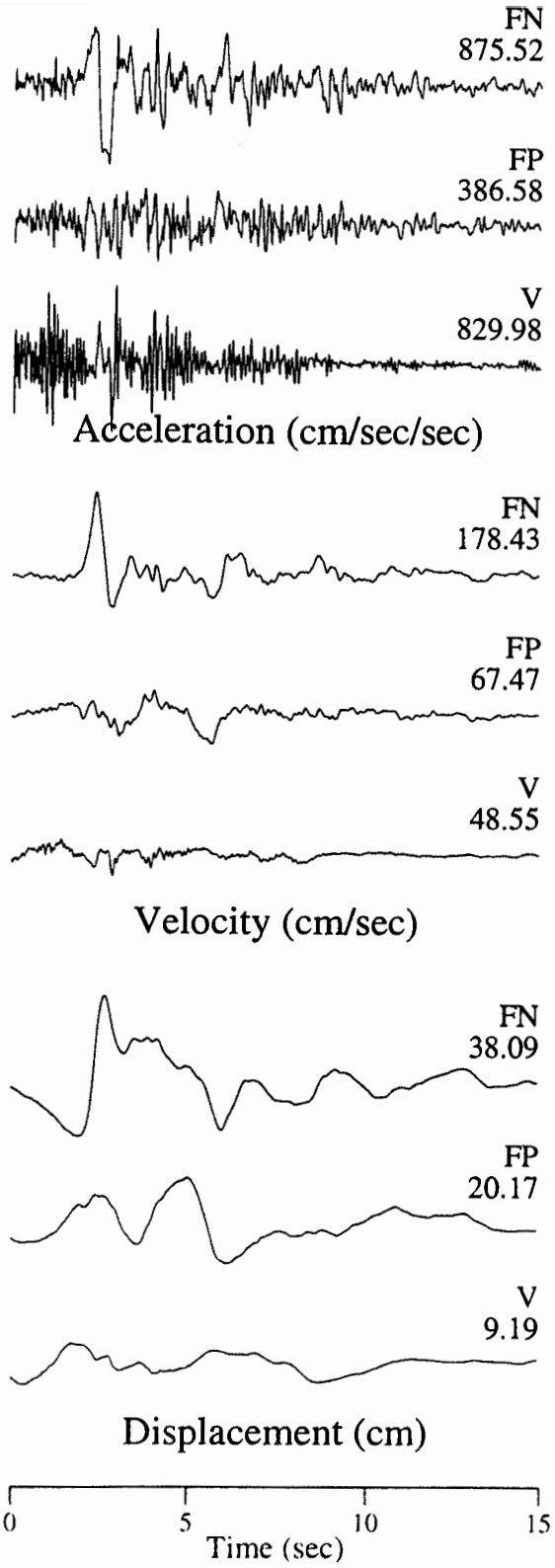

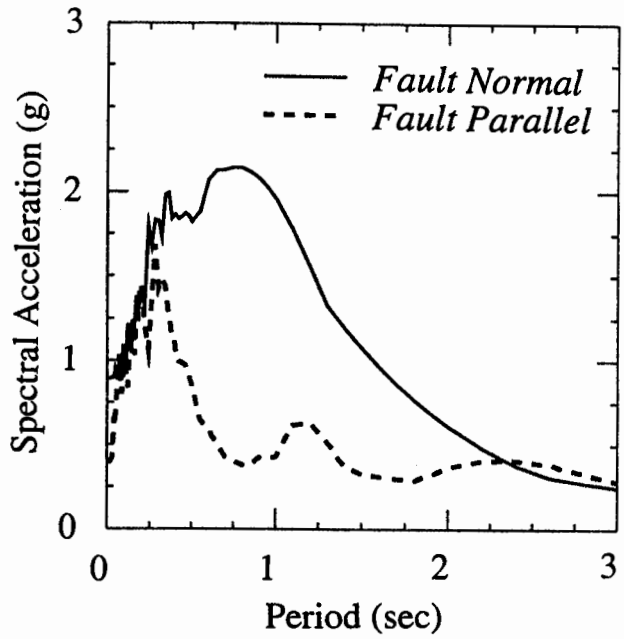

Figure 1. Acceleration and velocity time histories for the strike-normal and strike-parallel horizontal components of ground motion, and their 5% damped response spectra, recorded at Rinaldi during the 1994 Northridge earthquake.

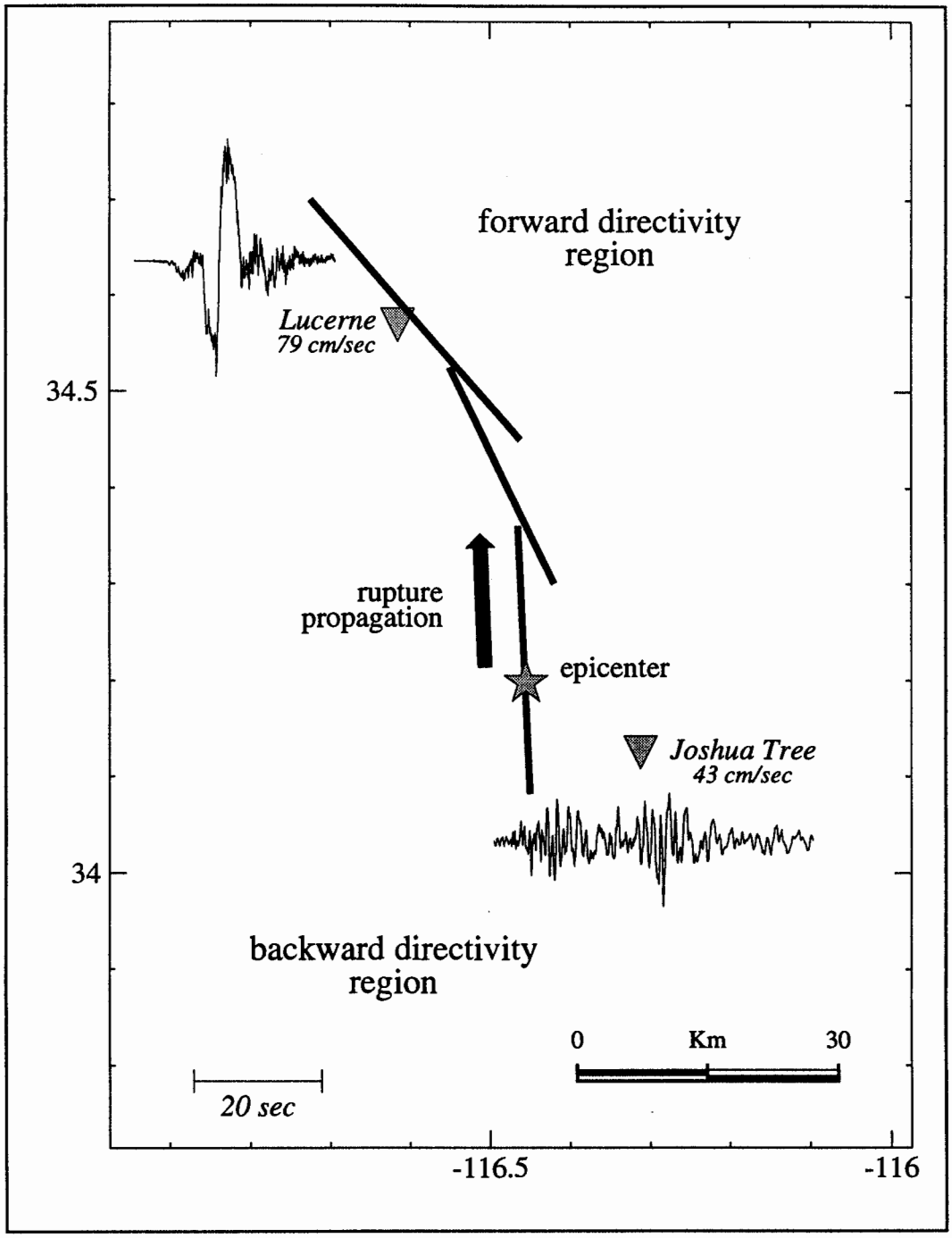

Figure 2. Map of the Landers region showing the location of the rupture of the 1992 Landers earthquake (which occurred on three fault segments), the epicenter, and the recording stations at Lucerne and Joshua Tree. The strike normal velocity time histories at Lucerne and Joshua Tree exhibit forward and backward rupture directivity effects respectively.

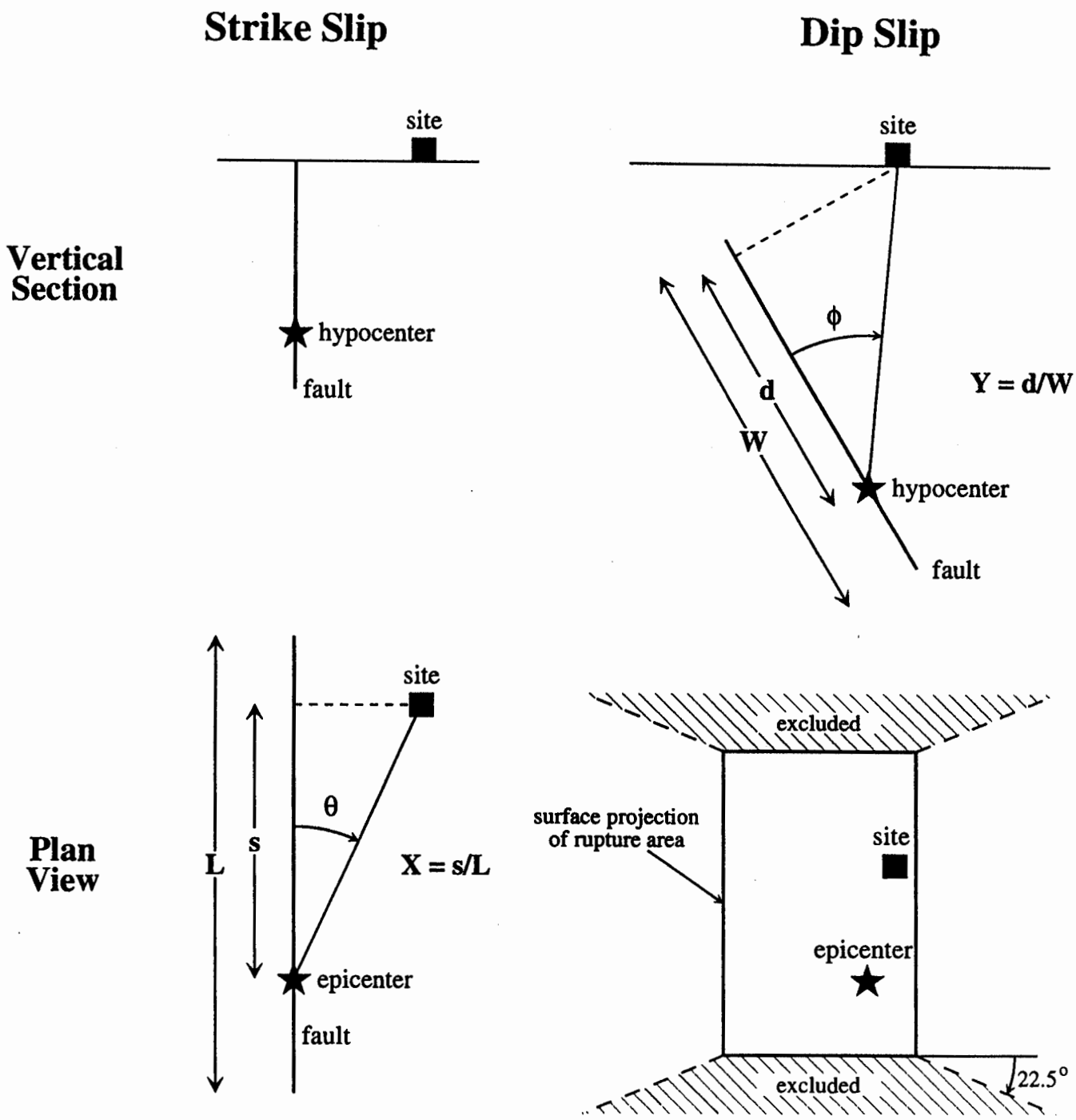

Figure 3. Definition of rupture directivity parameters θ and X for strike-slip faults, and ϕ and Y for dip-slip faults, and region off the end of dip-slip faults excluded from the model.

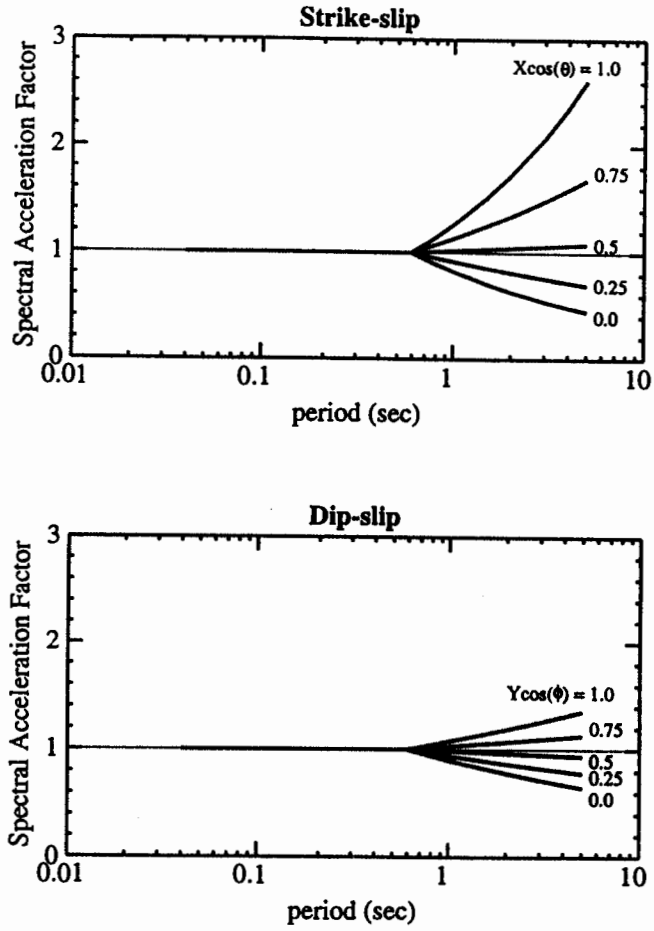

Figure 4a. Empirical model of the response spectral factor, showing its dependence on period and on the directivity function (X cos θ for strike-slip; Y cos ϕ for dip-slip)

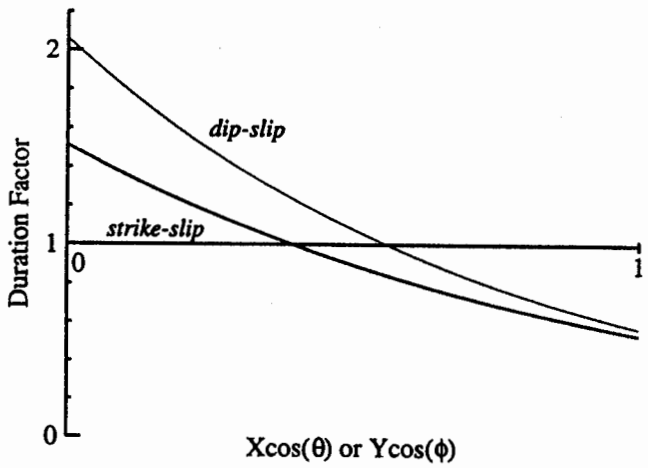

Figure 4b. Empirical model of the duration factor, showing its dependence on the directivity function (X cos θ for strike-slip; Y cos ϕ for dip-slip).

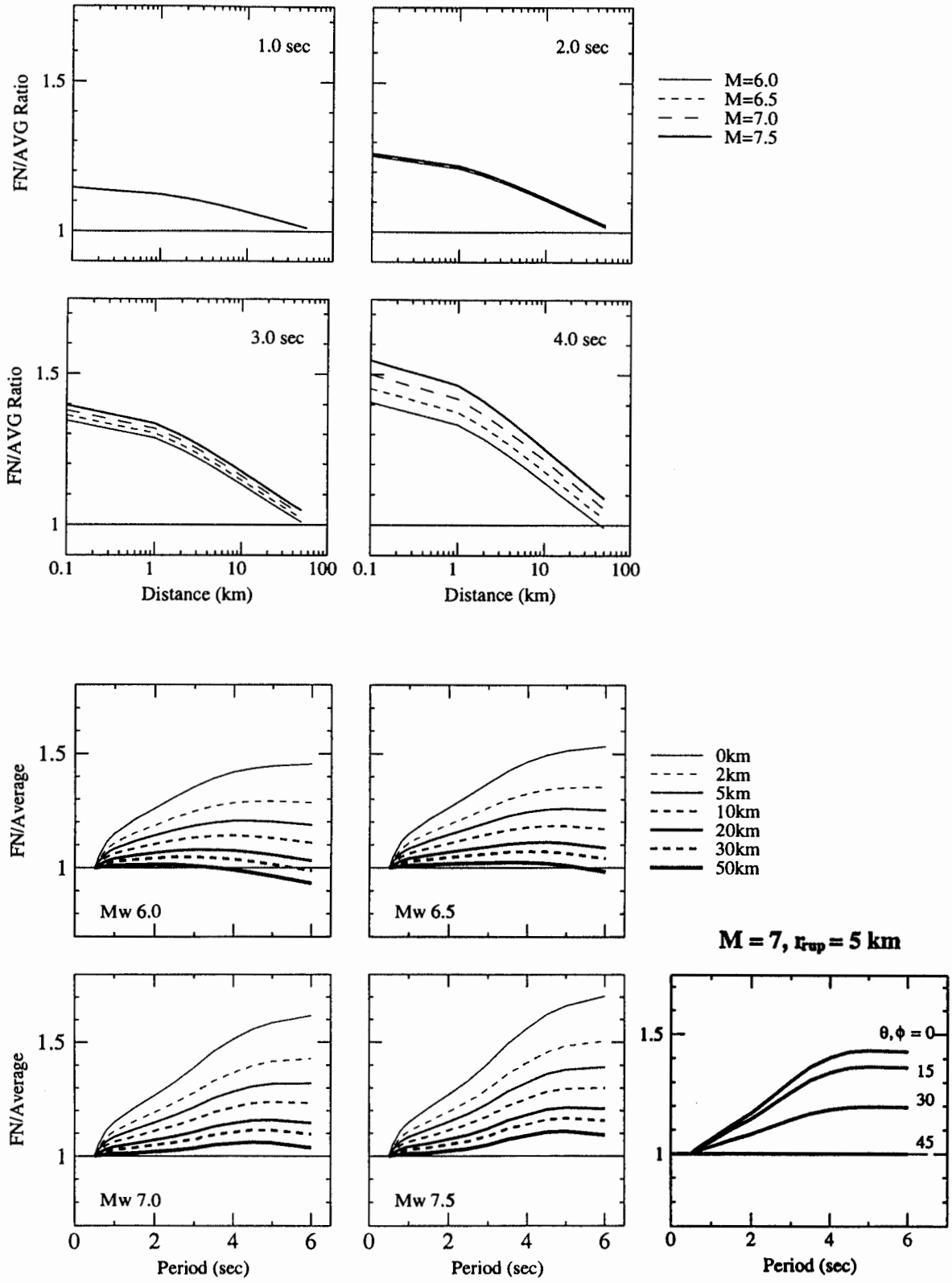

Figure 5. Empirical model of the strike-normal to average horizontal response spectral ratio excluding dependence on the angles θ or ϕ, shown as a function of period for various magnitudes and distances (top), and as function of distance for various magnitudes and periods (bottom). The dependence on angle θ or ϕ for M = 7 and r_{rup} = 5 km is shown as a function of period on the bottom right.

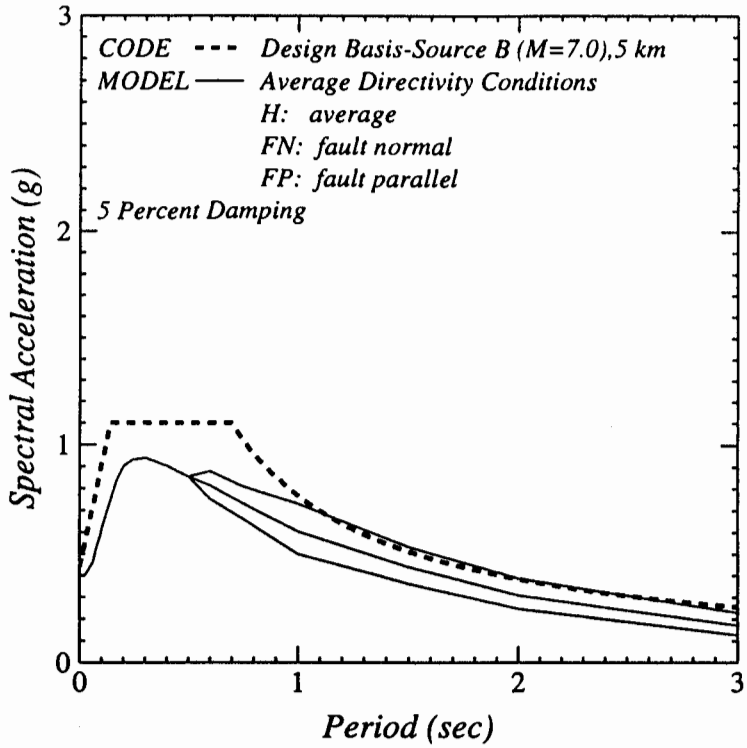

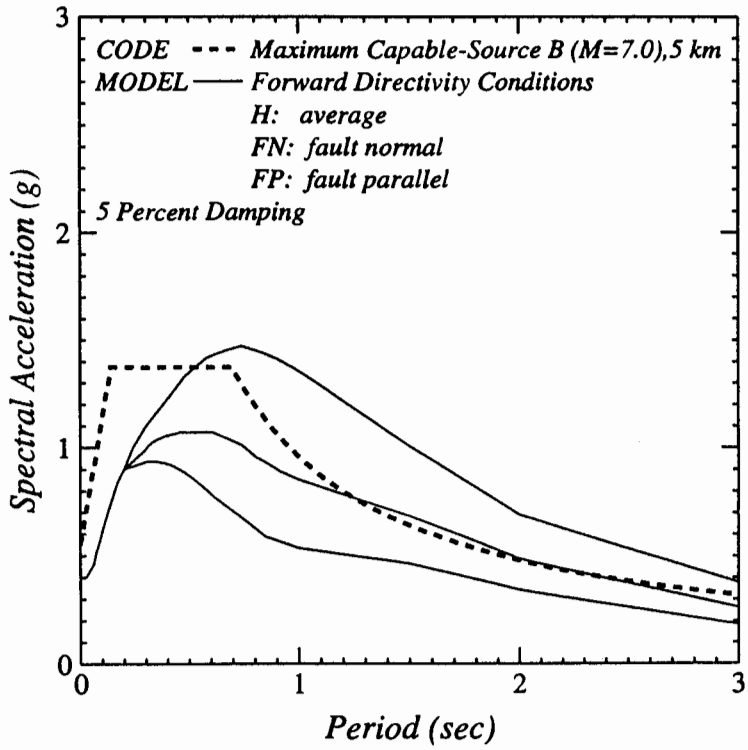

Figure 6. Response spectra for (top) average rupture directivity conditions and (bottom) forward rupture directivity conditions for a magnitude 7 earthquake at a distance of 5 km on soil. The response spectra are shown for the strike-normal, strike-parallel, and average horizontal components. Also shown for comparison are UBC spectra including the near-fault factor for design basis (top) and maximum capable (bottom) events.

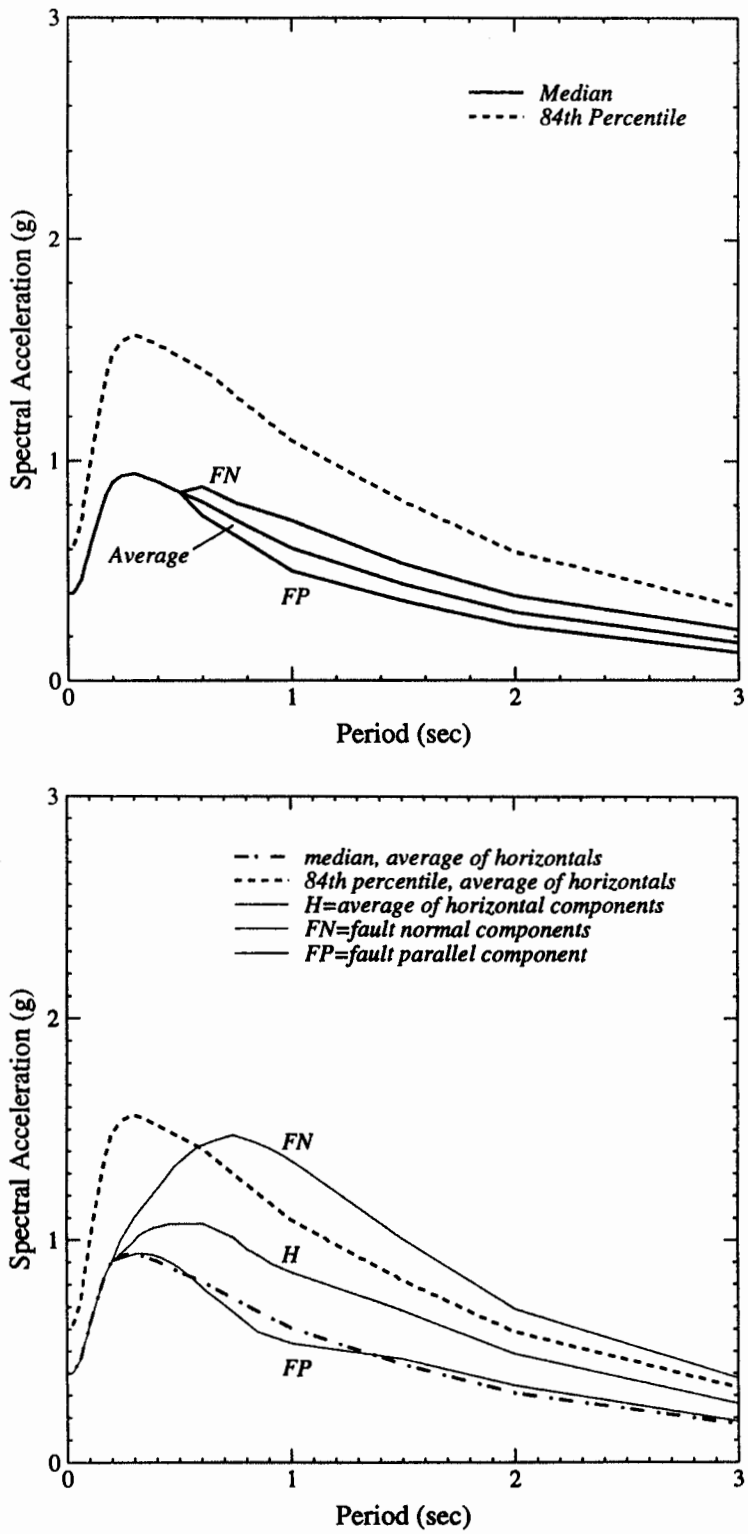

Figure 7. Response spectra for (top) average rupture directivity conditions and (bottom) forward rupture directivity conditions for a magnitude 7 earthquake at a distance of 5 km on soil. The response spectra are shown for the strike-normal, strike-parallel, and average horizontal components. Also shown for comparison are the median and 84th percentile spectra for the empirical attenuation relation (Abrahamson and Silva, 1997) on which the modifications for near-fault effects are based.

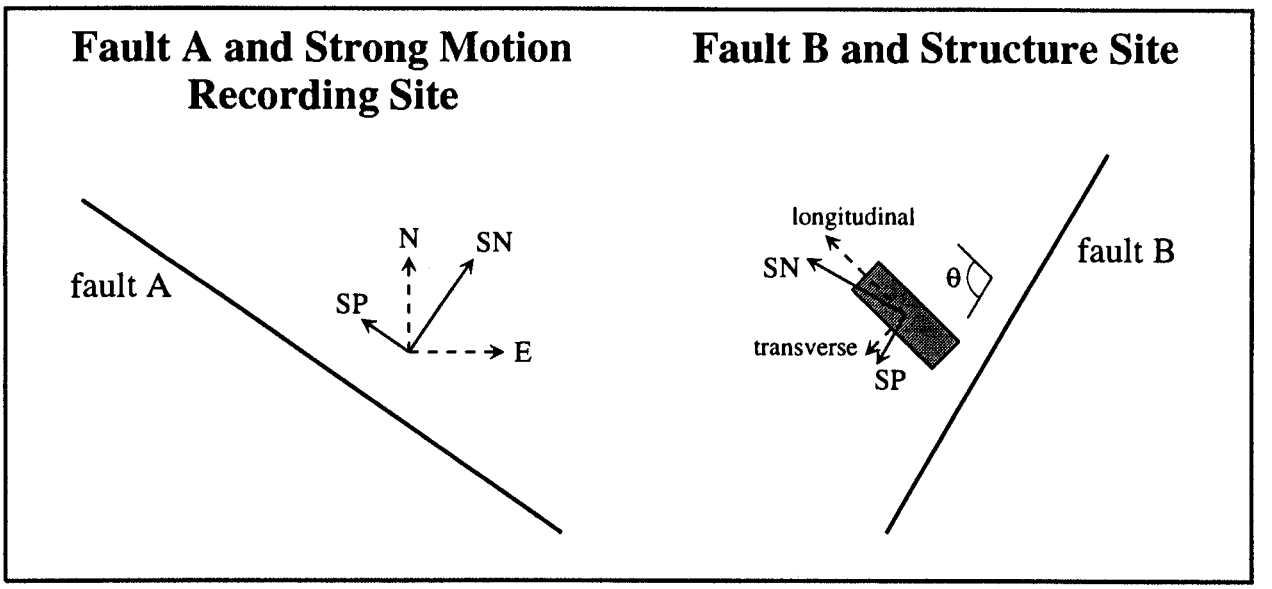

Figure 8a. Schematic diagram of the orientation of ground motion at a recording site, its rotation into strike-normal and strike-parallel components, transfer to a structure site in that orientation, and rotation into longitudinal and transverse components of the structure.

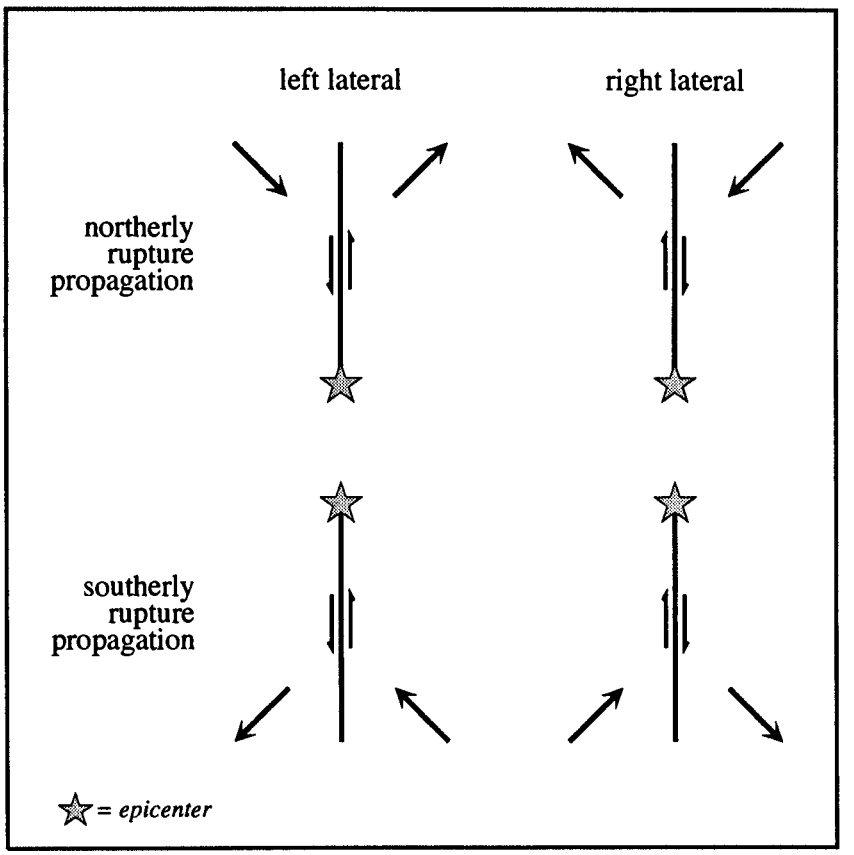

Figure 8b. Schematic diagram of the polarity of permanent ground displacement for strike-slip earthquakes. The motions are shown for both left-lateral and right-lateral unilateral faults, and for both northerly and southerly rupture propagation on north-striking faults.